arXiv:1403.7638v1 [cond-mat.str-el] 29 Mar 2014

# Spin-dependent beating patterns in thermoelectric properties: filtering the carriers of the heat flux in a Kondo adatom system

A. C. Seridonio[1,2], E. C. Siqueira[2], R. Franco[3], J. Silva-Valencia[3], I. A. Shelykh[4,5], and M. S. Figueira[6]
[1] *Instituto de Geociências e Ciências Exatas - IGCE, Universidade Estadual Paulista, Departamento de Física, 13506-970, Rio Claro, SP, Brazil*
[2] *Departamento de Física e Química, Universidade Estadual Paulista, 15385-000, Ilha Solteira, SP, Brazil*
[3] *Departamento de Física, Universidad Nacional de Colombia, A. A. 5997, Bogotá, Colombia*
[4] *Division of Physics and Applied Physics, Nanyang Technological University 637371, Singapore*
[5] *Science Institute, University of Iceland, Dunhagi-3, IS-107, Reykjavik, Iceland*
[6] *Instituto de Física, Universidade Federal Fluminense, 24210-340, Niterói, RJ, Brazil*

We theoretically investigate the thermoelectric properties of a spin-polarized two-dimensional electron gas hosting a Kondo adatom hybridized with an STM tip. Such a setup is treated within the single-impurity Anderson model in combination with the atomic approach for the Green's functions. Due to the spin dependence of the Fermi wavenumbers the electrical and thermal conductances, together with thermopower and Lorenz number reveal beating patterns as function of the STM tip position in the Kondo regime. In particular, by tuning the lateral displacement of the tip with respect to the adatom vicinity, the temperature and the position of the adatom level, one can change the sign of the Seebeck coefficient. This opens a possibility of the microscopic control of the heat flux analogously to that established for the electrical current.

PACS numbers: 72.10.Fk, 07.79.Fc, 85.75.-d, 72.25.-b

## I. INTRODUCTION

In the last few years, the fascinating field of thermoelectric properties of nano-scale materials is attracting the growing attention from both experimental[1–7] and theoretical[8–11] communities of researchers. In this context, Y. Dubi and M. Di Ventra[12] have recently proposed a fundamental setup: two leads connected by a nanoscopic region, in which thermodynamic quantities such as temperature can be tuned. The possible examples are quantum dot embedded inside a ballistic channel or a molecule efficiently coupled to both substrate and STM tip[7,13]. The main goal is to achieve a microscopic control of the heat flux analogously to that performed for the electrical current. Such a task was accomplished in the hybrid S-I-N-I-S materials[6], where S stands for the superconducting leads, I for the insulating barriers and N for normal metal. In this device, the heat is carried by the hottest electrons that flow towards the superconductors causing the cooling of the metallic region. The heat flux is controlled by the voltage applied to an extra lead and it can be increased, decreased or kept constant just by changing this voltage similarly to what is done with electrical current through an ordinary transistor.

Additionally, novel effects are manifested in the presence of ferromagnetic leads[14–26] and long spin-relaxation time[27,28] when thermoelectric properties become spin-dependent. In this case the spin degeneracy of the chemical potentials is lifted and the phenomenon known as spin accumulation arises, drastically affecting the behavior of the thermoelectric quantities.

Another setup promising for the control of thermoelectric flux consists of scanning tunneling microscopy break junction (STMBJ)[7,29]. In this geometry, molecules are trapped between an STM tip of Au kept at the room temperature $T$ and a substrate of the same material having different temperature $T + \Delta T$. Molecular junctions are created by moving the STM tip towards the surface of the metallic electrode and when the circuit is closed, a bias-voltage is applied and the current is measured.

In the aforementioned systems, the dynamics is ruled by the laws of quantum mechanics, thus leading to wave phenomena analogously to those observed in classical mechanics. In particular, we highlight the so-called beating effect, which is due to the interference between two waves that propagate in the same direction with equal amplitudes and slightly different frequencies and wavenumbers. Beating effects routinely appear in condensed matter physics. As an example they can be detected by using of the technique of Faraday rotation in CdSe quantum dots: the Zeeman splitting produces a beating pattern in the spin magnetization[30]. Similar feature is also present in a device composed by two quantum dots coupled to source and drain leads[31]. In such a system, oscillatory gate voltages characterized by slightly different frequencies are attached to these dots and produce beating pattern in the current signal. Additionally, the appearance of the beats in STM setups has been recently detected in the $NbS_3$ one-dimensional conductor[32,33].

In this work we focus on the theoretical study of the thermoelectric properties of spin-polarized two-dimensional electron gas (2DEG) hosting a Kondo adatom coupled to an STM tip as sketched in Fig. 1. The setup is treated by using the single-impurity Anderson Hamiltonian[34] and the atomic approach[35,36] for the Green's functions, in which the STM tip and the "host+adatom" systems play, respectively, the roles of the cold and hot reservoirs. In the framework of the linear response theory, when voltage and temperature gradients are small, we derive analytical expressions for the

thermoelectric coefficients characterizing the system. We find that in the Kondo regime these quantities as functions of the STM tip position exhibit beating patterns, which are due to the dependence of Fermi wavenumbers of the host on spin. We show that in the regime of large Fano factor[37,38], the thermopower (Seebeck coefficient) alternates its sign by changing the following degrees of freedom: the lateral separation of the STM tip with respect to the adatom, the temperature and the position of the adatom level. It is worth mentioning that to tune the adatom level with respect to the host Fermi energy, we consider in the model an AFM tip capacitively coupled to this adatom, thus allowing one to control the position of its energy level as originally proposed by some of us in Ref. [39]. The cases of presence and absence of the spin accumulation phenomenon are considered. In both of them, positive and negative signs imply that the carriers responsible for heat conductance are electrons and holes, respectively. Thus we show in this work that the system outlined in Fig. 1 operates as a filter of the carriers responsible for the heat conductance.

To our best knowledge, experimental data are not available for the device we consider. However, the standard procedure used in the STMBJ experiments should allow easy experimental verification of our predictions. It is worth mentioning that STMBJ device usually operates under room temperature, which could be an obstacle for the implementation of such a technique in Kondo regime required for the emergence of the beats. On the other hand, the magnitudes of $T_K$ for adatoms are higher with respect to those found in quantum dots and lie within the range $50\text{K} \lesssim T_K \lesssim 100\text{K}$[40], and thus the observation of the beating patterns in thermoelectric coefficients should not be very complicated experimentally.

This paper is organized as follows: in Sec. II, we develop the theoretical model for the system sketched in Fig. 1 as well as the derivation of the expressions for thermoelectric coefficients and the Green's function of the Kondo adatom. The results are present in Sec. III and in Sec. IV, we summarize our concluding remarks.

## II. THEORETICAL MODEL

The system we investigate (see Fig.1) is described by the following Hamiltonian

$$\mathcal{H}_{\text{total}} = \mathcal{H}_{\text{host}} + \mathcal{H}_{\text{tip}} + \mathcal{H}_{\text{tun}}, \tag{1}$$

where $\mathcal{H}_{\text{host}}$ corresponds to the host electrons in 2DEG and adatom, $\mathcal{H}_{\text{tip}}$ to the STM tip and $\mathcal{H}_{\text{tun}}$ to the tip-host hybridization. In frameworks of the single-impurity

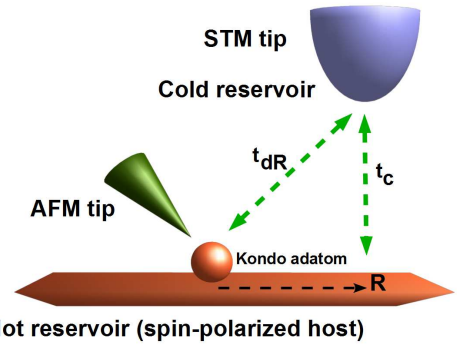


Figure 1. STM device composed by a normal tip (cold reservoir) and a Kondo adatom hybridized with a spin-polarized two-dimensional electron gas (hot reservoir). The parameters $t_{\text{dR}}$ and $t_{\text{c}}$ correspond to the hopping terms in the Hamiltonian. In Kondo regime, the thermoelectric properties characterized by the electrical and thermal conductances, the thermopower (Seebeck coefficient) and Lorenz number entering into the Wiedemann-Franz law exhibit beating patterns if STM tip is displaced laterally with respect to the adatom position. An AFM tip capacitively coupled to the adatom is required as previously proposed in Ref. [39] to tune its energy level.

Anderson model[34] the terms in Eq. (1) read:

$$\begin{aligned}\mathcal{H}_{\text{host}} = &\sum_{\vec{k}\sigma} \varepsilon_{k\sigma} c^{\dagger}_{\vec{k}\sigma} c_{\vec{k}\sigma} + E_d \sum_{\sigma} d^{\dagger}_{\sigma} d_{\sigma} \\ &+ V \sum_{\vec{k}\sigma} (c^{\dagger}_{\vec{k}\sigma} d_{\sigma} + \text{H.c.}) + U d^{\dagger}_{\uparrow} d_{\uparrow} d^{\dagger}_{\downarrow} d_{\downarrow}. \end{aligned} \tag{2}$$

Here the electrons in the host are described by the operator $c^{\dagger}_{\vec{k}\sigma}$ ($c_{\vec{k}\sigma}$) for the creation (annihilation) of an electron in a quantum state labeled by the wave number $\vec{k}$ with an energy

$$\varepsilon_{k\sigma} = \frac{\hbar^2 k^2}{2m} - D_{\sigma}, \tag{3}$$

where $D_{\sigma} = D(1 + \sigma P)$, $D$ is the band half-width in the absence of spin polarization, $P$ is polarization degree of the host defined as

$$P = \frac{\rho^{\uparrow}_{\text{host}} - \rho^{\downarrow}_{\text{host}}}{\rho^{\uparrow}_{\text{host}} + \rho^{\downarrow}_{\text{host}}}, \tag{4}$$

where $\rho^{\sigma}_{\text{host}}$ are spin dependent densities of states. According to the Stoner criteria of itinerant magnetism[19], $-D_{\sigma} \leq \varepsilon_{k\sigma} \leq D(1 - \sigma P)$. For the adatom, $d^{\dagger}_{\sigma}$ ($d_{\sigma}$) creates (annihilates) an electron in the state $E_d$. Parameter $V$ describes the hybridization of the adatom with 2DEG. The last term in Eq. (2) accounts for the on-site Coulomb interaction $U$.

The Hamiltonian of the tip corresponds to the free electrons described by fermionic operators $b^{\dagger}_{\vec{q}\sigma}$ and $b_{\vec{q}\sigma}$ and reads:

$$\mathcal{H}_{\rm tip} = \sum_{\vec{q}\sigma} \varepsilon_q b^{\dagger}_{\vec{q}\sigma} b_{\vec{q}\sigma}. \tag{5}$$

The tunneling Hamiltonian can be expressed as:

$$\mathcal{H}_{\rm tun} = t_c \sum_{\vec{q}\sigma} b^{\dagger}_{\vec{q}\sigma} \psi^{\sigma}_{R} + \text{H.c.}, \tag{6}$$

where $t_c$ is the STM tip-host coupling,

$$\psi^{\sigma}_{R} = \sum_{\vec{k}} \phi_{\vec{k}}(\vec{R}) c_{\vec{k}\sigma} + (\pi\Delta\rho_0)^{1/2} q d_{\sigma} \tag{7}$$

is the field operator that accounts for the Fano interference of the tip to 2DEG and tip to adatom paths, $\phi_{\vec{k}}(\vec{R}) = e^{i\vec{k}.\vec{R}}$, $\Delta = \pi V^2 \rho_0$ is the Anderson parameter and $q$ is the Fano factor of the STM device. The latter can be expressed as:

$$q = q_0 e^{-k_F R}, \tag{8}$$

where $k_F$ is the Fermi wave number of the host in the case $P = 0$ and $R$ is a lateral distance between the tip and the host. Note that according to the Eqs. (7) and (8), the limit $q_0 \gg 1$ represents the situation in which the tip is highly hybridized with the adatom, while in the opposite regime $q_0 \ll 1$, the tip is strongly connected to the surface [see Fig. 1]. Naturally, the increase of the distance between the tip and adatom leads to the quenching of the coupling between them, and for $k_F R \gg 1$ the Fano parameter drops to zero.

### A. Thermoelectric coefficients

By applying the linear response theory, and treating tip to host coupling term $\mathcal{H}_{\rm tun}$ perturbatively, it is possible to show that in absence of spin accumulation the thermoelectric coefficients[11,41,42] are given by the following expressions:

$$G = G_{\uparrow} + G_{\downarrow} = e^2 \sum_{\sigma} I_{o\sigma}, \tag{9}$$

and

$$\kappa = \frac{1}{T}\left( \sum_{\sigma} I_{2\sigma} - \frac{\left(\sum_{\sigma} I_{1\sigma}\right)^2}{\sum_{\sigma} I_{o\sigma}} \right) \tag{10}$$

for the electrical and thermal conductances, respectively, and

$$S = S_{\uparrow} + S_{\downarrow} = -\frac{1}{eT} \frac{\sum_{\sigma} I_{1\sigma}}{\sum_{\sigma} I_{o\sigma}} \tag{11}$$

for the Seebeck coefficient (thermopower), $e > 0$ stands for the electron charge. To calculate the transport coefficients $I_o$, $I_1$, and $I_2$, we follow the paper of B. Dong and X. L. Lei[8]:

$$I_{n\sigma} = \frac{1}{h} \int \left( -\frac{\partial n_F}{\partial \omega} \right) \omega^n \tau_{\sigma}(\omega, R) d\omega, \tag{12}$$

with

$$\tau_{\sigma}(\omega, R) = \tau_b \rho^{\sigma}_{\rm LDOS}(\omega, R), \tag{13}$$

where $h$ is the Planck constant, $n_{\rm F}$ stands for the Fermi-Dirac distribution, $\tau_{\sigma}(\omega, R)$ is the spin-dependent transmittance, $\rho^{\sigma}_{\rm LDOS}(\omega, R)$ is the spin-polarized local density of states (LDOS) of the "host+adatom" system at the position $\vec{R}$ in the host surface and $\tau_b = D/(1+q^2)$.

For the case of spin accumulation, which is characterized by the lifting of the spin degeneracy in the chemical potentials of the leads, the expressions for the thermal conductance and thermopower should be modified[27,28]:

$$\bar{\kappa} = \bar{\kappa}_{\uparrow} + \bar{\kappa}_{\downarrow} = \frac{1}{T} \sum_{\sigma} \left( I_{2\sigma} - \frac{I^2_{1\sigma}}{I_{o\sigma}} \right) \tag{14}$$

and

$$\bar{S} = \bar{S}_{\uparrow} + \bar{S}_{\downarrow} = -\frac{1}{2eT} \sum_{\sigma} \frac{I_{1\sigma}}{I_{o\sigma}}. \tag{15}$$

Notice that differently from the case in which there is no spin accumulation the thermal conductance can be represented as sum of the terms corresponding to spin up and down channels (compare Eq. (14) and Eq.(10)).

According to the Wiedemann-Franz (WF) law in ordinary metals, the ratio between the electronic contribution to the thermal conductance $\kappa$ and the temperature $T$ times the electrical conductance $G$ known as Lorenz ratio,

$$L \equiv \frac{\kappa(T)}{TG(T)}, \tag{16}$$

is an universal value[11], $L = L_0 = (\frac{\pi^2}{3})(\frac{k_B}{e})^2$, where $k_B$ is the Boltzmann constant and $e$ is the electron charge. In our calculations, the ratio above differs from $L_0$ and together with conductance and Seebeck coefficient reveal beating patterns as function of tip-adatom separation.

In order to obtain the LDOS necessary for the calculation of thermoelectric coefficients, it is convenient to define the retarded Green's function for the field operator in Eq. (7), which in time domain reads:

$$\mathcal{R}^{\sigma}_{\psi_R\psi_R}(t) = -\frac{i}{\hbar}\theta(t)\, \mathtt{Tr}\{\varrho[\psi^{\sigma}_{R}(t), \psi^{\sigma\dagger}_{R}(0)]_{+}\}, \tag{17}$$

where $\theta(t)$ is the Heaviside function, $\mathtt{Tr}$ stands for the trace over the Hamiltonian states, $\varrho$ is the density matrix of the system described by the Hamiltonian [Eq. (2)] and $[\cdots,\cdots]_+$ stands for the anticommutator. From Eq. (17), the LDOS of the host can be obtained as

$$\rho^{\sigma}_{\mathrm{LDOS}}(\omega,R)=-\frac{1}{\pi}\mathtt{Im}(\tilde{\mathcal{R}}^{\sigma}_{\psi_R\psi_R}), \tag{18}$$

where $\tilde{\mathcal{R}}^{\sigma}_{\psi_R\psi_R}$ is the Fourier transform of $\mathcal{R}^{\sigma}_{\psi_R\psi_R}(t)$.

To determine an analytical expression for the LDOS, we apply the equation-of-motion approach. Placing Eq. (7) into Eq. (17), one gets:

$$\begin{aligned}\mathcal{R}^{\sigma}_{\psi_R\psi_R}(t)=&\sum_{\vec{k}\vec{q}}\phi_{\vec{k}}(\vec{R})\phi^{*}_{\vec{q}}(\vec{R})\mathcal{R}^{\sigma}_{c_{\vec{k}}c_{\vec{q}}}+(\pi\Delta\rho_0)q^2\mathcal{R}^{\sigma}_{dd}\\&+(\pi\Delta\rho_0)^{1/2}q\sum_{\vec{k}}[\phi^{*}_{\vec{k}}(\vec{R})\mathcal{R}^{\sigma}_{dc_{\vec{k}}}+\phi_{\vec{k}}(\vec{R})\mathcal{R}^{\sigma}_{c_{\vec{k}}d}],\end{aligned} \tag{19}$$

which depends on the Green's functions $\mathcal{R}^{\sigma}_{c_{\vec{k}}c_{\vec{q}}}$, $\mathcal{R}^{\sigma}_{dc_{\vec{k}}}$, $\mathcal{R}^{\sigma}_{c_{\vec{k}}d}$ and $\mathcal{R}^{\sigma}_{dd}$. First, we have to find

$$\mathcal{R}^{\sigma}_{c_{\vec{k}}c_{\vec{q}}}(t)=-\frac{i}{\hbar}\theta(t)\,\mathtt{Tr}\{\varrho[c_{\vec{k}\sigma}(t),c^{\dagger}_{\vec{q}\sigma}(0)]_+\} \tag{20}$$

by acting the operator $\partial_t\equiv\partial/\partial t$ on Eq. (20). We obtain

$$\begin{aligned}\partial_t\mathcal{R}^{\sigma}_{c_{\vec{k}}c_{\vec{q}}}(t)=&-\frac{i}{\hbar}\delta(t)\,\mathtt{Tr}\{\varrho[c_{\vec{k}\sigma}(t),c^{\dagger}_{\vec{q}\sigma}(0)]_+\}\\&-\frac{i}{\hbar}\varepsilon_k\mathcal{R}^{\sigma}_{c_{\vec{k}}c_{\vec{q}}}(t)-\frac{i}{\hbar}V\mathcal{R}^{\sigma}_{dc_{\vec{q}}}(t),\end{aligned} \tag{21}$$

where we used that

$$i\hbar\partial_t c_{\vec{k}\sigma}(t)=[c_{\vec{k}},\mathcal{H}_{\mathrm{host}}]=\varepsilon_k c_{\vec{k}\sigma}+Vd_\sigma(t). \tag{22}$$

In the energy domain $\omega$, we solve Eq. (21) for $\tilde{\mathcal{R}}^{\sigma}_{c_{\vec{k}}c_{\vec{q}}}$ and obtain

$$\tilde{\mathcal{R}}^{\sigma}_{c_{\vec{k}}c_{\vec{q}}}=\frac{\delta_{\vec{k}\vec{q}}}{\varepsilon^{+}-\varepsilon_k}+\frac{V}{\varepsilon^{+}-\varepsilon_k}\tilde{\mathcal{R}}^{\sigma}_{dc_{\vec{q}}}, \tag{23}$$

where $\varepsilon^{+}=\omega+i\eta$ and $\eta\to0^{+}$. Notice that we also need to calculate the mixed Green's function $\tilde{\mathcal{R}}_{dc_{\vec{q}}}$. Analogously, we find

$$\tilde{\mathcal{R}}^{\sigma}_{dc_{\vec{q}}}=\frac{V}{\varepsilon^{+}-\varepsilon_q}\tilde{\mathcal{R}}^{\sigma}_{dd}=\tilde{\mathcal{R}}^{\sigma}_{c_{\vec{q}}d}. \tag{24}$$

Now within the wide band limit $D\to\infty$, we place Eq. (24) into Eq. (23) and then substitute these equations back into Eqs. (18) and (19). This procedure results into the following expression for the spin-polarized LDOS of the system:

$$\begin{aligned}\rho^{\sigma}_{\mathrm{LDOS}}(\omega,R)=&\rho^{\sigma}_{\mathrm{host}}+\rho_0\Delta[(\mathcal{F}^2_\sigma-q^2)\mathtt{Im}(\tilde{\mathcal{R}}^{\sigma}_{dd})\\&+2\mathcal{F}_\sigma q\mathtt{Re}(\tilde{\mathcal{R}}^{\sigma}_{dd})]\end{aligned} \tag{25}$$

where

$$\mathcal{F}_\sigma=\frac{1}{\rho_0}\sum_{\vec{k}}\phi_{\vec{k}}(\vec{R})\delta(\varepsilon-\varepsilon_{k\sigma})=\frac{\rho^{\sigma}_{\mathrm{host}}}{\rho_0}J_0(k_{\mathrm{F}\sigma}R) \tag{26}$$

accounts for the Friedel oscillations described by the *zeroth* order Bessel function $J_0$ dependent on the spin-dependent Fermi wavenumbers as follows:

$$k_{\mathrm{F}\downarrow}=\sqrt{\frac{1-P}{1+P}}k_{\mathrm{F}\uparrow}. \tag{27}$$

Additionally, to determine the LDOS, we need to find the Green's function $\tilde{\mathcal{R}}^{\sigma}_{dd}$ of the adatom. In the present work it is obtained via the atomic approach in the limit of infinite on-site Coulomb interaction.

### B. The atomic approach

In order to implement the atomic approach for the case of the infinite Coulomb energy[35,36], we begin with Eq. (2) expressed as

$$\begin{aligned}\mathcal{H}_{\mathrm{host}}=&\sum_{\vec{k}\sigma}\varepsilon_{k\sigma}c^{\dagger}_{\vec{k}\sigma}c_{\vec{k}\sigma}+E_d\sum_{\sigma}X_{d,\sigma\sigma}\\&+V\sum_{\vec{k}\sigma}(c^{\dagger}_{\vec{k}\sigma}X_{d,0\sigma}+\mathrm{H.c.}),\end{aligned} \tag{28}$$

where $X_{p,ab}=|p,a\rangle\langle p,b|$ is the Hubbard operator that projects out the doubly occupied state from the adatom to ensure the limit of infinite Coulomb correlation, the label $(a,b)$ defines the parameters associated with the corresponding atomic transition. This formalism is based on an extension of the Hubbard cumulant expansion also applicable to the Anderson lattice with impurity-host couplings treated as perturbations. The use of this expansion allows one to express the exact Green's function in terms of an unknown effective cumulant. In previous works[35,36], we have studied the Anderson lattice with an approximate effective cumulant obtained from the atomic limit of the model in a procedure that we call the zero band width (ZBW) approximation. The advantage is that such a method includes all the higher order cumulants absent in our previous diagrammatic calculations.

To obtain the exact Green's function of the adatom, we can employ the chain approximation considering all the possible cumulants in the expansion for the Anderson lattice. Similarly to what is done for the Feynman diagrams, it is possible to rearrange all of those cumulant diagrams that contribute to the exact adatom Green's function by defining an effective cumulant, determined by all the diagrams that cannot be separated by cutting a single edge ("proper" or "irreducible" diagrams).

As we are interested in the exact Green's function for the adatom, we use the standard definition

$$\mathcal{R}^{\sigma}_{dd}(t)=-\frac{i}{\hbar}\theta(t)\,\mathtt{Tr}\{\varrho[d_\sigma(t),d^{\dagger}_{\sigma}(0)]_+\}. \tag{29}$$

The Fourier transformation of Eq. (29) over time coordinate provides the adatom Green's function in energy domain, which is then obtained by replacing the bare cumulant by the effective one calculated by following the atomic approach with the Hamiltonian in Eq. (28). As a result, we have

$$\tilde{\mathcal{R}}^{\sigma}_{dd}(\omega) = \frac{\mathcal{M}^{\sigma}_{\rm eff}(\omega)}{1 - \mathcal{M}^{eff}_{\sigma}(\omega)|V|^2 \sum_{\vec{k}} \tilde{\mathcal{R}}^{\sigma}_{c}(\vec{k},\omega)}, \tag{30}$$

for the adatom Green's function in terms of the effective cumulant $\mathcal{M}^{\sigma}_{\rm eff}(\omega)$ and the free-electron Green's function

$$\tilde{\mathcal{R}}^{\sigma}_{c}(\vec{k},\omega) = \frac{1}{\omega - \varepsilon_{\vec{k}\sigma} + i\eta}, \tag{31}$$

where $\eta \to 0^{+}$. The atomic version of Eq. (30) is given by:

$$\tilde{\mathcal{R}}^{\sigma}_{dd,\rm at}(\omega) = \frac{\mathcal{M}^{\sigma}_{\rm at}(\omega)}{1 - \mathcal{M}^{\sigma}_{\rm at}(\omega)|V|^2 \tilde{\mathcal{R}}^{\sigma}_{\rm ZBW}(\omega)}, \tag{32}$$

which results in

$$\mathcal{M}^{\sigma}_{\rm at}(\omega) = \frac{\tilde{\mathcal{R}}^{\sigma}_{dd,\rm at}(\omega)}{1 + \tilde{\mathcal{R}}^{\sigma}_{dd,\rm at}(\omega)|V|^2 \tilde{\mathcal{R}}^{\sigma}_{\rm ZBW}(\omega)}, \tag{33}$$

for the effective cumulant determined from the adatom Green's function, both dependent on

$$\tilde{\mathcal{R}}^{\sigma}_{\rm ZBW}(\omega) = \frac{1}{\omega - (\varepsilon_{0\sigma} - \mu) + i\eta}, \tag{34}$$

for an electron state, in the ZBW approximation with $\mu$ as the chemical potential of the host. As one can see, Eq. (34) replaces all energy contributions of the original Fermi sea by two spin dependent atomic levels, i.e., one can perform the substitution $\sum_{\vec{k}\sigma} \varepsilon_{k\sigma} c^{\dagger}_{\vec{k}\sigma} c_{\vec{k}\sigma} \to \sum_{\sigma} \varepsilon_{0\sigma} c^{\dagger}_{0\sigma} c_{0\sigma}$ in Eq. (28) with $\varepsilon_{k\sigma} = \varepsilon_{0\sigma}$ representing the band atomic level for a given spin $\sigma$. The ZBW overestimates the conduction electrons contribution concentrating them at a single energy level $\epsilon_{0\sigma}$, and to moderate this effect we shall replace $V^2$ by $\Delta^2$ in Eqs. (32) and (33), where $\Delta = \pi V^2 \rho_0$ is the Anderson parameter.

To determine the adatom Green's function, we use the atomic cumulant $\mathcal{M}^{\sigma}_{\rm at}(\omega)$ in Eq. (30) and verify that

$$\tilde{\mathcal{R}}^{\sigma}_{dd}(\omega) = \frac{\mathcal{M}^{\sigma}_{\rm at}(\omega)}{1 - \mathcal{M}^{\sigma}_{\rm at}(\omega)\dfrac{|V|^2}{2D} \ln\left[\dfrac{\omega - D(1-\sigma P) + \mu}{\omega + D(1+\sigma P) + \mu}\right]} \tag{35}$$

provides an analytical expression in the flat band approximation.

As the final step we have to find the proper values of the effective atomic levels $\varepsilon_{0\sigma}$ that well describe the ZBW Green's functions in Eq. (34) and consequently, the adatom Green's function. To that end, we use the condition that in metallic systems the most important region in the energy range for conduction electrons is

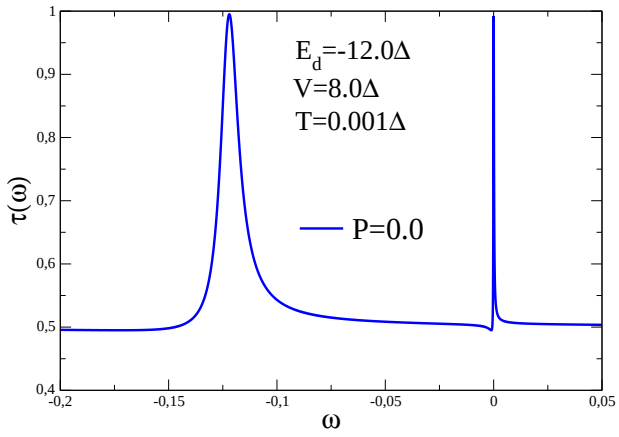


Figure 2. (Color online) The plot of total transmittance $\tau(\omega) = \tau_{\uparrow}(\omega, R=0) + \tau_{\downarrow}(\omega, R=0)$ entering into Eq. (13) as function of $\omega$. In Kondo regime it exhibits two characteristic peaks that reach the maximum value: the resonance due to the localized level $E_d$ in the domain $\omega < 0$ and Kondo peak situated at the chemical potential $\omega = \mu = 0$ of the host. The minimum of the transmittance occurs off the resonances, it decays to the background contribution of 1/2. The values of the parameters are: $q_0 = 10$, $P = 0$ (non magnetic host), $E_d = -12\Delta$, $V = 8.0\Delta$ and $T = 0.001\Delta$.

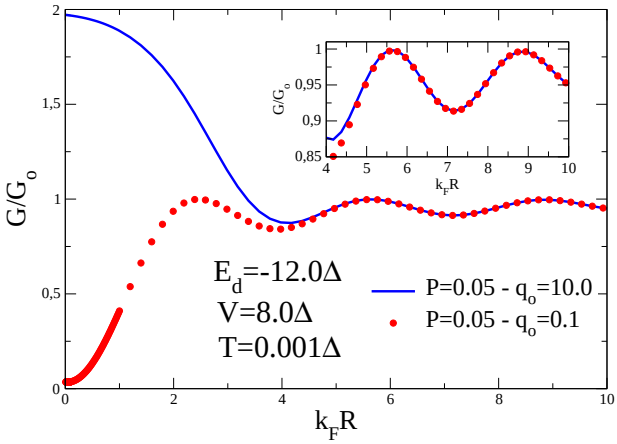


Figure 3. (Color online) (a) Electrical conductance $G$ as function of tip-adatom separation in Fano-Kondo regime. For $q_0 = 10$ constructive Fano interference combined with Kondo effect leads to the appearance of the conductance maximum at $k_F R = 0$. Contrastingly, in the case of $q_0 = 0.10$ the Fano interference is destructive, which leads to the conductance minimum at $k_F R = 0$. In both cases, Friedel oscillations are clearly seen for finite values of $k_F R$ and reveal universal pattern independent on $q$ as it is shown at the inset. The values of the parameters are $P = 0.05$ (ferromagnetic hosts), $E_d = -12\Delta$, $V = 8.0\Delta$ and $T = 0.001\Delta$.

located at the chemical potential $\mu$ and that the Friedel's sum rule is satisfied[43] for the adatom spectral density:

$$\rho_{d,\sigma}(\mu) = -\frac{1}{\pi}\mathrm{Im}[\tilde{\mathcal{R}}^{\sigma}_{dd}(\mu)] = \frac{\sin^2[\delta_\sigma(\mu)]}{\pi\Delta_\sigma}, \qquad (36)$$

where $\delta_\sigma(\mu) = \pi n_{d,\sigma}$ is the conduction phase shift at the chemical potential, $\Delta_\sigma = \Delta(1+\sigma P)$ is the spin-dependent Anderson parameter and $n_{d,\sigma}$ is the spin dependent adatom occupation. We can thus calculate self-consistently the atomic levels $\varepsilon_{0\sigma}$ using Eq. (36) together with the relation

$$n_{d,\sigma} = \langle X_{d,\sigma\sigma}\rangle = -\frac{1}{\pi}\int_{-\infty}^{+\infty} n_F \mathrm{Im}(\tilde{\mathcal{R}}^{\sigma}_{dd,\mathrm{at}}(\omega))d\omega. \qquad (37)$$

We highlight that the present calculations via the Friedel's sum rule given by Eq. (36) gives a pair of solutions for each spin subspace. The physically relevant solution should be found by minimizing the Helmholtz free energy obtained from the mixed Green's function $\tilde{\mathcal{R}}_{dc_{\vec{q}}}$ of Eq. (24) as described in the Ref. [44]. The details of the procedure was already discussed by one of the authors of the present paper[35], where all relevant details can be found.

By employing the atomic approach, we can find the transmittance $\tau(\omega) = \tau_\uparrow(\omega, R=0) + \tau_\downarrow(\omega, R=0)$ (see Eq. (13)) as a function of the single particle energy $\omega$. For the case of the STM tip placed right above the adatom ($R=0$) the result is shown at Fig. 2. In the Kondo regime and for constructive Fano interference the transmittance exhibits two characteristic peaks: the resonant structure localized at the level $E_d = -12.0\Delta$ due to the adatom and the Kondo peak placed at the chemical potential $\omega = \mu = 0$ of the host. Moreover, the minimum value of the transmittance is 1/2 off the resonances, thus representing the background contribution arising from the conduction band of the metallic surface. This confirms that the atomic approach is a reliable technique to capture the many-body physics of the Kondo effect, which allows us to safely apply it to the analysis of the thermoelectric properties of the setup presented in the next section.

## III. RESULTS

In this section we present the results for thermoelectric coefficients characterizing the system keeping the values of the parameters used in Fig. 2 and shown in the corresponding caption.

In Fig. 3 we show the electrical conductance $G$ of Eq. (9) in units of $G_o = e^2/h$ as a function of $k_F R$. We compare the behaviors of $G$ for the same value of host polarization $P$ and two different values of Fano parameter $q_o = 10.0$ and $q_o = 0.1$. In the former case, the electrical conductance at $k_F R$=0 remains close to $G/G_o = 2$, since the STM device acts as a single electron transistor[45,46]. On the other hand, for $q_o = 0.1$ due to the destructive

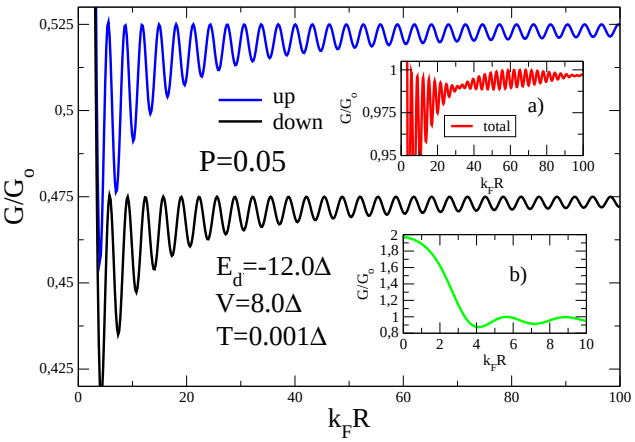


Figure 4. (Color online) Spin-resolved electrical conductances $G_\uparrow$ and $G_\downarrow$ in the Kondo regime as function of tip-adatom separation. Due to the non-zero polarization of the host ($P = 0.05$) the conductance in spin-up channel is bigger than the conductance in spin-down channel. Both channels reveal spin dependent Friedel oscillations. The used parameters are: $q_0 = 10$, $P = 0.05$ (ferromagnetic host), $E_d = -12\Delta$, $V = 8.0\Delta$ and $T = 0.001\Delta$. The insets for $G = G_\uparrow + G_\downarrow$ show the regime of the large distances where beating pattern is clearly observed (inset (a)) and small distances, where this pattern is absent (inset (b)).

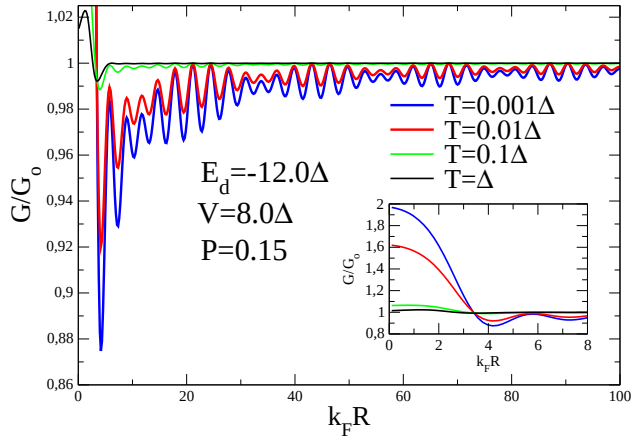


Figure 5. (Color online) Total conductance as function of the adatom-tip separation presented for different values of the temperature. For temperatures above Kondo temperature the beating pattern is suppressed. The inset shows the behavior of the conductance for small tip-adatom separations. The used values of the parameters are: $q_0 = 10$, $P = 0.05$ (magnetic host), $E_d = -12\Delta$ and $V = 8.0\Delta$.

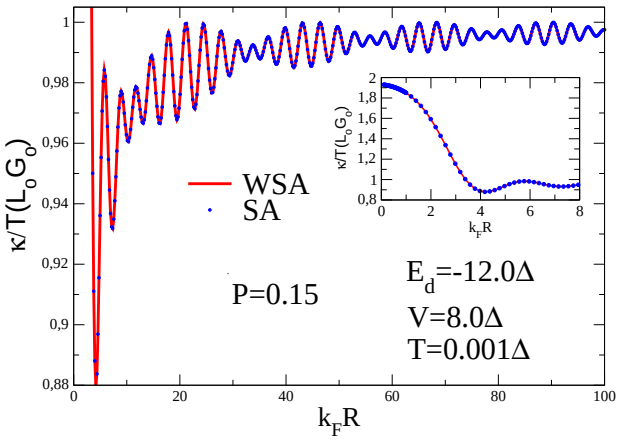


Figure 6. (Color online) Thermal conductance $\kappa$ in the Kondo regime as function of tip-adatom separation. Both cases of the absence of spin accumulation (denoted as WSA) and the presence of spin accumulation (denoted as SA) are presented and show very similar behavior. The used parameters are: $q_0 = 10$, $E_d = -12\Delta$, $V = 8.0\Delta$, $T = 0.001\Delta$ and $P = 0.15$ (ferromagnetic hosts).

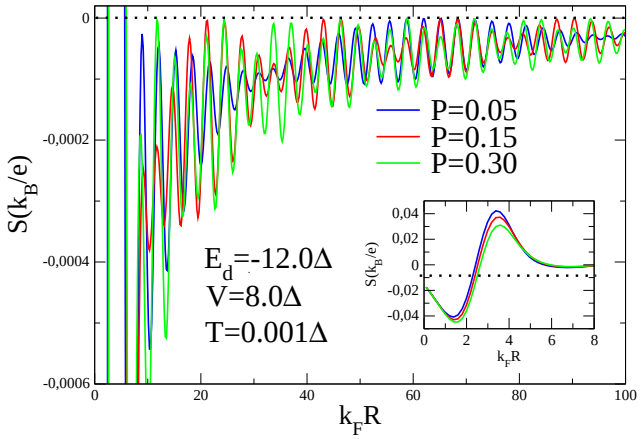


Figure 7. (Color online) Seebeck coefficient (thermopower) $S = S_\uparrow + S_\downarrow$ in the Kondo regime as function of tip-adatom separation for different values of the polarization of the host. The inset shows the behavior of $S$ for small tip-adatom separations, where $S$ exhibits the alternation of a sign. The heat flux is transmitted mainly by electrons in the region $S < 0$ and mainly by holes in the region $S > 0$. The used parameters are: $q_0 = 10$, $E_d = -12\Delta$, $V = 8.0\Delta$, $T = 0.001\Delta$ and different values of the spin-polarization $P$ (ferromagnetic hosts).

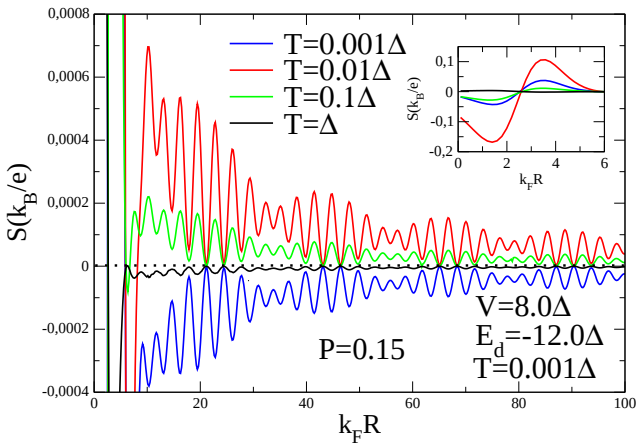


Figure 8. (Color online) Seebeck coefficient (thermopower) $S = S_\uparrow + S_\downarrow$ in the Kondo regime as function of tip-adatom separation for different values of the temperature, which allows one to change the sign of the thermopower and thus to control the type of the carriers responsible for the heat flux. The inset shows the behavior of $S$ for small tip-adatom separations. The used values of the parameters are: $q_0 = 10$, $E_d = -12\Delta$, $V = 8.0\Delta$, $P = 0.15$ (ferromagnetic hosts).

interference the electrical conductance is completely suppressed in analogy to that observed in T-shaped quantum dots[47]. For $k_F R > 4$, spin-polarized Friedel oscillations manifest, their shape is independent on $q$ and is ruled exclusively by the polarization $P$ as it is shown at the inset of Fig. 3.

To better understand the spin-polarized Friedel oscillations, we split the electrical conductance $G$ into spin resolved parts $G_\uparrow$ and $G_\downarrow$ as it is displayed in Fig. 4 for $P = 0.05$. As one can see the spin-up component is shifted towards higher values of $G$ and spin-down component moves in the opposite direction. This is due the spin-dependence of LDOS entering into Eqs. (9), (12) and (13). The difference in the Fermi wavenumbers for spin-up and spin-down electrons $k_{F\uparrow}$ and $k_{F\downarrow}$ results in a slight difference of the frequencies of the oscillations for spin resolved components of the conductance, which leads to the onset of the beating pattern in the total conductance shown at the inset (a) in the region of large tip-adatom separations. In the range of small distances between adatom and STM tip, such a feature does not emerge as it is seen at the inset (b).

In Fig. 5 we present the electrical conductance $G/G_o$ of Eq. (9) as a function of $k_F R$ with $P = 0.05$ and $q_o = 10$ for different temperatures $T$. The plot reveals that the beating pattern only appears at temperatures below the Kondo temperature $T_K$. As it was discussed in introduction, the characteristic values of $T_K$ lie in the range $50K \lesssim T_K \lesssim 100K$ and this regime is thus easily accessible experimentally. The inset of Fig. 5, shows

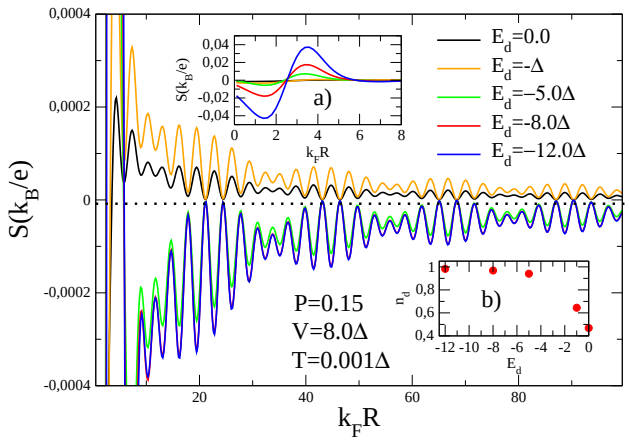


Figure 9. (Color online) Seebeck coefficient (thermopower) $S = S_\uparrow + S_\downarrow$ in the Kondo regime as function of tip-adatom separation for different values of energy of the adatom level $E_d$, which can be tuned by employing an AFM tip capacitively coupled to the adatom as proposed in Ref. [39]. Varying the value of $E_d$ one observes a crossover from the intermediate valence regime towards the Kondo limit, which results in the onset of a pronounced oscillation of Seebeck coefficient in the region of small tip-adatom separations shown at the inset (a). Inset (b) shows that the adatom occupation number $n_d = n_{d\uparrow} + n_{d\downarrow}$ determined by Eq. (37) attains the unitary limit as a hallmark that the system is within the Kondo regime for $E_d = -12.0\Delta$. Parameters used are: $q_0 = 10$, $V = 8.0\Delta$, $T = 0.001\Delta$, $P = 0.15$ (ferromagnetic hosts).

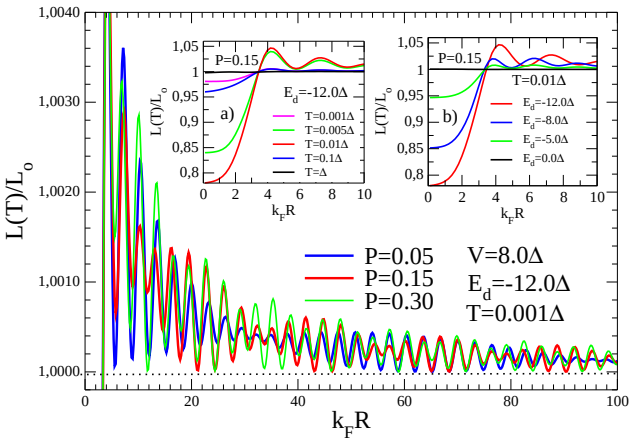


Figure 10. (Color online) Lorenz ratio in the Kondo regime as function of tip-adatom separation for different values of spin polarization. The main plot clearly demonstrates the deviation of the Lorenz number from its standard value $L_o = (\frac{\pi^2}{3})(\frac{k_B}{e})^2$ and reveals clear beating pattern. Used parameters are: $q_0 = 10$, $V = 8.0\Delta$, $T = 0.001\Delta$, $E_d = -12.0\Delta$, $P = 0.15$ (ferromagnetic hosts). The inset (a) shows $L$ for small tip-adatom separations for different values of the temperature for which deviation from Wiedemann-Franz law is most clearly seen. The inset (b) shows $L$ for small tip-adatom separations for different values of the adatom energy $E_d$ revealing the crossover from the extreme Kondo limit at $E_d = -12.0\Delta$ towards the intermediate valence regime characterized at $E_d = 0$.

.

the behavior of the electrical conductance for small tip-adatom separations. One can clearly see that Kondo effect dominates the tunneling through the adatom leading to the enhancement of the conductance. As temperature increases Kondo effect disappears and the conductance reaches the value given by the background contribution from the host surface.

Fig. 6 shows the thermal conductances of Eqs. (10) and (14) measured in the units of $L_0 G_0 T$, where $L_o = (\frac{\pi^2}{3})(\frac{k_B}{e})^2$ stands for the Lorenz number entering into Wiedemann-Franz law for the normal metals. We consider both cases of absent and present spin accumulation and show that for $P = 0.15$ the results are almost the same in both situations. To illustrate this feature, one can show that the thermal conductances follow the relationship

$$\kappa - \bar{\kappa} \sim P^2, \tag{38}$$

which is negligible for small polarizations values. In the same way, other thermoelectric properties exhibit similar behavior.

Fig. 7 shows the thermopower (Seebeck coefficient) $S$ of Eq. (11) as a function of $k_F R$, for different values of spin-polarization $P$ for the host. The sign of the thermopower allows one to determine the type of the carriers responsible for the heat conductance: for $S < 0$ they are electrons while for $S > 0$ they are holes. In the range of large tip-adatom separations Seebeck coefficient demonstrates a beating pattern in full analogy to the electrical and thermal conductances. In the region of small tip-adatom separations (shown at the inset) where Kondo effect becomes dominant the sign of $S$ changes. As a result, one can tune the type of carrier responsible for the heat conductance just by displacing laterally the STM tip from the adatom site. Therefore, in the Kondo regime the STM device can be used as filter for carriers of the heat flux.

In Fig. 8 we show the dependence of $S(k_F R)$ for different values of the temperature. For very low temperatures ($T = 0.001\Delta$), the corresponding beating pattern is governed by the Kondo effect and remains negative in the region of large tip-adatom separations (electrons as thermal carriers). Notably, increasing the temperature up to $T = 0.01\Delta$, the thermopower coefficient inverts its sign (holes becoming the thermal carriers). For high temperatures (green curve for $T = 0.1\Delta$), the Kondo effect vanishes (see the inset of the conductance of Fig. 5) and the beating pattern in the thermopower remains positive. For $T = \Delta$ (see the black curve), the sign of the

thermopower becomes negative being characterized by unpronounced amplitudes. As a result, the STM apparatus can also be employed as a filter of the heat carriers by changing the system temperature. The behavior of the thermopower in the range of small tip-adatom separations is illustrated in the inset of Fig. 8, where we can see a similar behavior in the corresponding inset of Fig. 7.

In Fig. 9 we present the thermopower $S$ of Eq. (11) as function of $k_F R$ for different values of the adatom level $E_d$ and fixed spin-polarization $P$. By tuning $E_d$ from the intermediate valence regime, characterized by $E_d = 0.0$ and $E_d = -\Delta$ ($S > 0$, holes as thermal carriers), towards the Kondo regime ($E_d = -5.0\Delta$, $E_d = -8.0\Delta$ and $E_d = -12.0\Delta$) ($S < 0$, electrons as thermal carriers), we demonstrate that one can control the type of carriers responsible for the heat conductance. The inset (a) shows the behavior of $S$ in the region of small tip-adatom separations, where the oscillatory pattern arising from the Kondo effect is observed for corresponding values of $E_d$. The inset (b) shows that the adatom occupation number $n_d = n_{d\uparrow} + n_{d\downarrow}$, determined by Eq. (37), approaches the unitary limit, thus confirming that the system is within the Kondo limit when $E_d = -12.0\Delta$.

In Fig. 10 we plot the value of Lorenz number entering into Wiedemann-Franz (WF) law (Eq. (16)) in the Kondo regime in units of the Lorenz number for normal metals $L_o = (\frac{\pi^2}{3})(\frac{k_B}{e})^2$ as function of $k_F R$. Similar to other thermoelectric coefficients, $L$ reveals characteristic beating pattern. At large distances between the tip and the adatom the amplitude of the beating approaches unity. The inset (a) shows the behavior of $L$ for small tip-adatom separations. One clearly sees that $L/L_0 \neq 1$ and thus the WF law is violated. The difference of the Lorenz number from the standard value becomes most pronounced for $T \approx 0.01\Delta$. The fulfillment of the WF law is recovered again when the temperature is increased. The violation of the WF law becomes most pronounced in the Kondo regime, when $E_d = -12.0\Delta$ and $T = 0.01\Delta$, as it is shown in the inset (b). This is a striking result and has been discussed recently in the literature[48–50]. The amplitude of the thermopower oscillation near the adatom presents a close relationship with the maximum violation of the WF law: the amplitude of $S$ is maximum, as indicated in the inset of Fig. 8, just at the temperature where the violation of the WF law is maximum as we can observe in the inset (b) of Fig. 10.

## IV. CONCLUSIONS

We have analyzed the beating patterns revealed by thermoelectric coefficients of the STM system and magnetic adatom on conducting surface. The beating patterns emerge at temperatures close to the Kondo temperature in the range of large tip-adatom separations. In this range, the beats are ruled exclusively by the spin-polarization degree of the ferromagnetic host. For small tip-adatom separations there is an extra dependence on the Fano parameter. Additionally, in this range we have demonstrated the violation of the Wiedemann-Franz law and sign-alternating behavior of the Seebeck coefficient $S$ in the Kondo regime. The possibility to tune the sign of $S$ opens a way to control the type of the carriers responsible for the heat transfer, as cases $S < 0$ and $S > 0$ correspond to electrons and holes, respectively. The technique of the scanning tunneling microscopy break junction (STMBJ)[7,29] is well established, and all our theoretical predictions can be verified experimentally.

## ACKNOWLEDGMENTS

This work was supported by the agencies CNPq, PROPe/UNESP, FP7 IRSES projects SPINMET and QOCaN. R. Franco and J. Silva-Valencia thanks to the ICTP-Trieste, where part of this work was done. A. C. Seridonio thanks the University of Iceland for hospitality.

[1] R. Scheibner, H. Buhmann, D. Reuter, M. N. Kiselev. L. W. Molemkamnp, Phys. Rev. Lett. **95**, 176602 (2005).
[2] R. Scheibner, E. G. Novik, T. Borzenko, M. König, D. Reuter, A. D. Wieck, H. Buhmann, L. W. Molenkamp, Phys. Rev. B. **75**, 041301 (2007).
[3] R. Scheibner, M. König, D Reuter, A. D. Wieck, C. Gould,H. Buhmann, and L. W. Molenkamp, New Journal of Physics, **10**, 083016 (2008).
[4] Eric A. Hoffmann, Henrik A. Nilsson, Jason E. Matthews, Natthapon Nakpathomkun, Ann I. Persson, Lars Samuelson and Heiner Linke, Nano Letters **9**, 779 (2009).
[5] C. W. Chang, D. Okawa, A. Mujumdar and A. Zettl, Science. **314**, 1121 (2006).
[6] Olli-Pentti Saira, M. Meschke, F. Giazotto, A. M. Savin, M. Möttonen, J. P. Pekola, Phys. Rev. Lett. **99**, 027203 (2007).
[7] Pramod Reddy, Sung-Yeon Jang, Rachel A. Segalman, and Arun Majumdar, Science. **315**, 1568 (2007).
[8] B. Dong and X. L. Lei, J. Phys. Condens. Matter. **14**, 11747 (2002).
[9] R. Franco, J. Silva-Valencia and M. S. Figueira, J. Mag. Mag. Mat. **320**, 242 (2008).
[10] M. Yoshida and L. N. Oliveira, Physica B. **404**, 3312 (2009).
[11] T. A. Costi and V. Zlatić, Phys. Rev. B. **81**, 235127 (2010).
[12] Yonatan Dubi and Massimiliano Di Ventra, Rev. of Mod. Phys. **83**, 131 (2011).
[13] Kanhayalal Baheti,Jonathan A. Malen,Peter Doak, Pramod Reddy, Sung-Yeon Jang,T. Don Tilley, Arun Majumdar, and Rachel A. Segalman, Nano Letters **8**, 715 (2008).
[14] S. L. Kawahara, J. Lagoute, C. Chacon, Y. Girard, J. Klein and S. Rousset, Phys. Rev. B **82** 020406R (2010).

[15] A. C. Seridonio, F. M. Souza, and I. A. Shelykh, J. Phys.: Condens. Matter **21**, 095003 (2009).
[16] A. C. Seridonio, F. M. Souza, J. Del Nero, and I. A. Shelykh, Physica E **41**, 1611 (2009).
[17] N. Néel, J. Kröger, and R. Berndt, Phys. Rev. B **82**, 233401 (2010).
[18] Y. Qi, J. X. Zhu, S. Zhang, and C. S. Ting, Phys. Rev. B **78** 045305 (2008).
[19] M. Sindel, L. Borda,J. Martinek, R. Bulla, J. König, G. Schön, S. Maekawa, and J. von Delft, Phys. Rev. B **76**, 045321 (2007).
[20] K. Hamaya, M. Kitabatake, K. Shibata, M. Jung, M. Kawamura, K. Hirakawa, T. Machida, and T. Taniyama, Appl. Phys. Lett. **91**, 232105 (2007).
[21] K. Hamaya, M. Kitabatake, K. Shibata, M. Jung, M. Kawamura, S. Ishida, T. Taniyama, K. Hirakawa, Y. Arakawa, and T. Machida, Phys. Rev. B **77**, 081302(R) (2008).
[22] M. R. Calvo, J. F. Rossier, J.J. Palacios, D. Jacob, D. Natelson, and C. Untiedt, Nature **458**, 1150 (2009).
[23] J. Hauptmann, J. Paaske, and P. Lindelof, Nature Phys. **4**, 373 (2008).
[24] I. Weymann, and L. Borda, Phys. Rev. B **81**, 115445 (2010).
[25] I. Weymann, Phys. Rev. B **83**, 113306 (2011).
[26] M. Misiorny, I. Weymann and J. Barnaś, Phys.Rev. Lett. **106**, 126602 (2011).
[27] R. Swirkowics, M. Wierzbicki, and J. Barnas, Phys. Rev. B. **80**, 195409 (2009).
[28] P. Trocha, and J. Barnas, Phys. Rev. B. **85**, 085408 (2012).
[29] Woochul Lee, Bai Song and Pramod Reddy, Annual Review of Heat Transfer, **Chapter 9**, 259 (2013).
[30] J. A. Gupta and D. D. Awschalom, X. Peng and A. P. Alivisatos, Phys. Rev. B. **59**, R10421 (1999).
[31] P. Trocha, Phys. Rev. B. **82**, 115320 (2010).
[32] Christophe Brun and Zhao-Zhong Wang and Pierre Monceau, Phys. Rev. B. **80**, 2045423 (2009).
[33] A. Prodan H.J.P. van Middena, R. Zitko, E. Zupanic, J.C. Bennett, H. Bohmc, Solid State Communications, **150** 2134 (2011).
[34] P. W. Anderson, Phys. Rev. **124**, 41 (1961).
[35] T. Lobo, M. S. Figueira and M. E. Foglio, Nanotechnology **17**, 6016 (2006).
[36] T. Lobo, M. S. Figueira and M. E. Foglio, Nanotechnology **21**, 274007 (2010).
[37] U. Fano, Phys. Rev. **124**, 1866 (1961).
[38] A. E. Miroshnichenko, S. Flach, and Y. S. Kivshar, Rev. Mod. Phys. **82**,2257 (2010).
[39] A. C. Seridonio, E. C. Siqueira, F. M. Souza, R. S. Machado, S. S. Lyra, and I. A. Shelykh, Phys. Rev. B **88**, 195122 (2013).
[40] P. Wahl, L. Diekhöner, M. A. Schneider, L. Vitali, G. Wittich, and K. Kern, Phys. Rev. Let. **93**, 176603 (2004).
[41] Gerald D. Mahan, *Many-Particle Physics*, second edition, Chap. **3**, pg. 227.
[42] J. M. Ziman, *Principles of the Theory of Solids*, second edition, chap. **7** pg. 229.
[43] J. Friedel, Adv. Phys. **3**, 446 (1954).
[44] S. Doniach and E. H. Sondheimer 1974 *Green's Functions for Solid State Physicists (New York: Benjamin)* (1974).
[45] D. Goldhaber-Gordon, H. Shtrikman, D. Mahalu, D. Abusch-Magder, U. Meirav, and M. A. Kastner, Nature **391**, 156 (1998).
[46] S. M. Cronenwett, T. H. Oosterkamp, and L. P. Kouwenhoven, Science **281**, 540 (1998).
[47] A. C. Seridonio, M. Yoshida, and L. N. Oliveira, Euro Phys. Lett. **86**, 67006 (2009).
[48] Bjorn Kubala, Jurgen Konig and Jukka Pekola, Phys. Rev. Lett. **100**, 066801 (2008).
[49] Piotr Trocha and Józef Barnás, Phys. Rev. B. **85**, 085408 (2012).
[50] G. Gómez-Silva, O. Ávalos-Ovando, M. L. Ladrón de Guevara, and P. A. Orellana, J. Appl. Phys. **111**, 053704 (2012).